P1.35 ADVANCES IN COMPRESSION OF ULTRASPECTRAL SOUNDER DATA

Bormin Huang*, Alok Ahuja, and Hung-Lung Huang
CIMSS, University of Wisconsin-Madison

Timothy J. Schmit and Roger W. Heymann
NOAA, National Environmental Satellite, Data, and Information Service

1. INTRODUCTION

In the era of contemporary and future ultraspectral sounders such as Atmospheric Infrared Sounder (AIRS) (Aumann et al. 2001), Cross-track Infrared Sounder (CrIS) (Bloom 2001), Infrared Atmospheric Sounding Interferometer (IASI) (Phulpin et al. 2002), Geosynchronous Imaging Fourier Transform Spectrometer (GIFTS) (Smith et al. 2002), and Hyperspectral Environmental Suite (HES) (Huang et al. 2003), better inference of atmospheric, cloud and surface parameters is feasible. An unprecedented amount of three-dimensional (3D) ultraspectral data, consisting of two spatial and one spectral dimension, is produced by the ultraspectral sounders. For example, the HES is the next-generation NOAA/NESDIS Geostationary Operational Environmental Satellite (GOES) sounder, slated for launch in 2013. It would be either a Michelson interferometer or a grating spectrometer, with high spectral resolution (over one thousand infrared channels with spectral widths on the order of 0.5 wavenumber), high temporal resolution (better than 1 hour), high spatial resolution (less than 10km) and hemispheric coverage. Given the large volume of 3D data that will be generated by an ultraspectral sounder each day, the use of robust data compression techniques will be beneficial to data transfer and archive.

There exist differences between ultraspectral sounder data and hyperspectral imager data in terms of application areas and subsequent user constraints on the data compression. The hyperspectral imager data (e.g. the well-known AVIRIS data (Abousleman 1999)) is in the visible or near-infrared regions with major application categories of anomaly detection, target recognition and background characterization (Shaw et al. 2003). Lossy compression is usually acceptable for imager data as long as the tolerance limits in application-specific metrics are met (Saghri et al. 1995). These metrics include those that signify scientific loss for end users (Qian et al. 2001; Ryan et al. 1998), content-independent metrics (Shen et al. 1993), and even visual comparisons (Eckstein et al. 2000). On the other hand, the ultraspectral sounder data is in the infrared region with the main purpose of retrieving atmospheric temperature, moisture and trace gases profiles, surface temperature and emissivity, cloud and aerosol optical properties for better weather and climate prediction. The physical retrieval of these geophysical parameters involves the inverse solution of the radiative transfer equation, and it is a mathematically ill-posed problem (Huang et al. 2002), i.e. the solution is sensitive to the error or noise in the data. Therefore there is a need for lossless or near-lossless compression of ultraspectral sounder data to avoid potential retrieval degradation of geophysical parameters due to lossy compression. Here, near-lossless compression implies that the error spectrum between the reconstructed data set and original data set to be significantly less than the sensor noise spectrum.

This paper presents advances in lossless compression of ultraspectral sounder data. The lossless compression schemes are divided into transform-based, prediction-based, and clustering-based schemes. The ultraspectral sounder data features strong correlations in disjoint spectral regions affected by the same type of absorbing gases at various altitudes. To take advantage of this fact, a bias-adjusted reordering (BAR) data preprocessing scheme (Huang et al. 2004c) is devised that is applicable to any 2D compression method. The rest of the paper is arranged as follows. Section 2 describes the ultraspectral sounder data used in this paper. Section 3 elaborates the BAR scheme while Section 4 highlights the different compression schemes along with their compression results. Section 5 summarizes the paper.

2. DATA

The ultraspectral sounder data could be generated from either a Michelson interferometer (e.g. CrIS, IASI and GIFTS) or a grating spectrometer (e.g. AIRS). Compression is performed on the standard ultraspectral sounder data set used before in (Huang et al. 2004a). It consists of ten granules, five daytime and five nighttime, selected from representative geographical regions of the Earth. Their locations, UTC times and local time adjustments are listed in Table 1. The data is publicly available via anonymous ftp (ftp://ftp.ssec.wisc.edu-/pub/bormin/Count).

This standard ultraspectral sounder data set adopts the NASA AIRS digital counts on March 2, 2004. The AIRS data includes 2378 infrared channels in the 3.74 to 15.4 μm region of the spectrum. A day's worth of AIRS data is divided into 240 granules, each of 6 minute

*Corresponding author address: Bormin Huang, 1225 W. Dayton St., Madison, WI 53706; e-mail: bormin@ssec.wisc.edu

durations. Each granule consists of 135 scan lines containing 90 cross-track footprints per scan line; thus there are a total of 135 x 90 = 12,150 footprints per granule. More information regarding the AIRS instrument may be acquired from the NASA AIRS website (http://www-airs.nasa.jpl.gov).

The digital count data ranges from 12-bit to 14-bit for different channels. Each channel is saved using its own bit depth. To make the selected data more generic to other ultraspectral sounders, 271 bad channels identified in the supplied AIRS infrared channel properties file are excluded, assuming that they occur only in the AIRS sounder. Each resulting granule is saved as a binary file, arranged as 2107 channels, 135 scan lines, and 90 pixels for each scan line. Figure 1 shows the AIRS digital counts at wavenumber 800.01cm^{-1} for the 10 selected granules on March 2, 2004. In these granules, coast lines are depicted by solid curves and multiple clouds at various altitudes are shown as different shades of colored pixels.

3. DATA PREPROCESSING SCHEME

For application of 2D compression schemes to the 3D ultraspectral sounder data, one can process the data framewise or make the data two-dimensional by converting the two spatial dimensions into one dimension by a continuous scan. The disadvantage to the first approach is that it does not explore the correlation between different spectral channels. The second approach is a better alternative for improving the spatial correlations among the neighboring pixels via the 2D compression schemes. Nevertheless, these 2D schemes do not explore the spectral correlations among the disjoint channels – a spectroscopic feature in the ultraspectral sounder data. To improve their compression on the ultraspectral sounder data, a bias-adjusted reordering (BAR) preprocessing scheme was proposed (Huang et al. 2004c) for converting the 3D data into 2D with the highest correlation channels rearranged together.

The BAR scheme takes advantage of the unique spectroscopic characteristic of ultrarspectral sounder data that features the strong correlations in disjoint spectral regions affected by the same type of absorbing gases at various altitudes. Figure 2 shows an example of the dominant absorption gases in different spectral regions. It can also explore the spatial correlations of disjoint geographical regions affected by the same type of absorbing gases or clouds. The BAR scheme is geared towards exploiting these correlations along different dimensions. When applying the BAR scheme in the spectral dimension, channels with similar dynamic range but different radiance values due to each channel's altitude preference are bias aligned together for finding the highest correlated spatial vector as the nearest neighbor of each reordered channel. Similarly, when applying the BAR scheme to the spatial dimension, pixels with similar dynamic range but different radiance values due to different amount of absorption from the same kind of absorption gases or clouds are bias aligned together for finding the highest correlated spectral vector as the nearest neighbor of each reordered pixel. A detailed explanation of the BAR scheme is given in Huang et al. (2004c). For 2D compression schemes, each granule with the size of 2107 channels by 135 scan lines by 90 footprints is converted into 2D with the size of 2107 channels by 12150 samples via the Boustrophedon pattern. Following these observations, compression gains have been reported on 3D SPIHT, JPEG2000, JPEG-LS and CALIC in Huang et al. (2004b).

The effects of the BAR scheme can be gauged by looking at the reordered 2D data patterns in the spectral-spatial domain. Figure 3 shows such an example for granule 82. Comparing Fig. 3(a) with Fig. 3(b), we can see that the data pattern is smoother along the spectral dimension after spectral reordering. This results in a higher compression ratio for Fig. 3(b). Similarly, the spatially reordered data in Fig. 3(c) is smoother than that in Fig. 3(a) along the spatial dimension. Fig 3(d) depicts the reordering along both dimensions that produces a smoother transition along both dimensions. Moreover, the bias adjustment has reduced the dynamic range of the reordered data as visualized by the reduction of grayscale intensities.

Figure 4 shows the sorting indices plotted against the original indices in the cases of spectral BAR for 4 granules. The sorting indices are quite different from the original indices as judged by their great deviation from the straight line. This shows the natural channel order given by the spectral wavelengths do not possess optimal correlation in neighboring channels. Another interesting fact is that in the BAR scheme, a given starting channel produces its own unique list of reordering indices and subsequently the compression ratios are different for different starting channels. An investigation of the effects of the starting channel has been conducted in Huang et al. (2004d). A noteworthy conclusion was that any starting channel may be used without compromising the compression ratio significantly.

4. COMPRESSION SCHEMES

4.1 Transform-based schemes

3D SPIHT with BAR: SPIHT (Said et al. 1996) is an embedded coding algorithm that performs bit-plane coding of the wavelet coefficients. It uses spatially oriented trees to describe the relationship between the parents on higher levels to the children and grandchildren on lower levels. It has low complexity and provides good performance. Extensions to 3D have been proposed in (Tang et al. 2003; Dragotti et al. 2000). Huang et al. (2003) presented a 3D SPIHT version to tackle irregular size 3D data, the dimensions of which need not be divisible by 2^N, where N is the levels of wavelet decomposition being performed. For application to ultraspectral sounder data, various 3D integer wavelet transforms were used followed by the 3D SPIHT method and arithmetic coding. The compression ratios obtained are shown in Fig. 5. As can

be seen, different choices of wavelet transforms produce different compression ratios. The compression gains using the spectral BAR preprocessing are evident in Fig. 6. The compression ratios obtained for all ten granules are significantly higher with spectral BAR followed by 3D SPIHT than using 3D SPIHT alone.

JPEG2000 with BAR: This algorithm is published as a new standard of ISO/IEC, as well as an ITU-T recommendation (ISO/IEC 2000). Its rich feature list includes progressive transmission by quality, resolution, component, or spatial locality, lossy and lossless compression, region of interest coding by progression, and limited memory implementations, to name a few. The JPEG2000 encoder consists of four main stages: discrete wavelet transform (DWT), scalar quantization, and two tiers of block coding, as depicted in Fig. 7. After the DWT stage, embedded scalar quantization is performed with the quantization step size possibly varying for each subband. The block coder is based on the principles of Embedded Block Coding with Optimized Truncation (EBCOT) (Taubman 2000) and includes an arithmetic coder coupled with a rate-distortion optimization algorithm to achieve the optimal bit rates. The performance of JPEG2000 compression with and without different reordering schemes on the ten granules is shown in Fig. 8. It is seen that all reordering schemes combined with JPEG2000 outperform JPEG2000 applied alone.

Lossless PCA: The Principal Component Analysis transform (PCA) or the Karhunen-Loève transform (KLT) has long been used in applications pertaining to hyperspectral images such as feature extraction, dimensionality reduction, and pattern recognition (Chang et al. 1999). PCA has also been used for lossy compression of hyperspectral imager data (Canta et al. 1998; Hoffman et al. 1994; Lee et al. 2000). We investigated PCA for lossless compression of the ultraspectral sounder data. PCA is a linear transform that utilizes the data statistics to construct an orthogonal basis on which the data is projected, and simultaneously decorrelated by diagonalization of the data covariance matrix. The advantage of using PCA is that it gives the smallest average error when approximating a data set by its projection on an orthogonal basis (Mallat 1999). To ensure lossless compression of the ultraspectral sounder data, the error residuals are rounded and entropy-coded. The compression ratios of the ten granules using lossless PCA with 60 PC's are shown in Table 2.

4.2 Prediction-based schemes

CALIC with BAR: The CALIC scheme (Wu 1997) is considered as the most efficient and complex encoder for compression of 2D continuous-tone images. Among the nine proposals in the initial ISO/JPEG evaluation in July 1995, CALIC was ranked first. It works on the principle of a context-adaptive non-linear predictor which adjusts to the local gradients around the current pixel. As shown in Fig. 7, the algorithm operates in the binary or continuous modes. The binary mode codes the regions of the image in which the intensity value is no more than two. In the continuous mode, the system has four major components: gradient-adjusted prediction, context selection and quantization, context modeling of prediction errors, and entropy coding of prediction errors. The compression ratios obtained by using CALIC with and without different BAR schemes are depicted in Fig. 10. A significant improvement in compression ratio is seen by using both BAR scheme with CALIC. Moreover, all schemes combining reordering with CALIC outperform CALIC alone.

JPEG-LS with BAR: The ISO/IEC working group released a new standard for the lossless/ near-lossless compression of continuous-tone images in 1999, popularly known as JPEG-LS (ISO/IEC 1999). It features low complexities based on predictive coding technique. Near-lossless compression is controlled through an integer valued threshold representing the maximum permissible absolute difference between each original pixel value and its decompressed value. Figure 11 shows the JPEG-LS encoder that is composed of four main stages: prediction, context modeling, error encoding, and run mode. In Fig. 12, the compression ratios of JPEG-LS with and without different reordering schemes on the ten granules are depicted. It is seen that all reordering schemes combined with JPEG-LS outperform JPEG-LS applied alone.

4.3 Clustering-based schemes

Partitioned Vector Quantization schemes: Vector Quantization (VQ) is a well-known technique for source coding. Despite its widespread use for hyperspectral imager data compression (Abousleman et al. 1997; Canta et al. 1998), one of the significant drawbacks towards its use is the computational complexity required in the codebook generation process. Many fast VQ algorithms have been proposed in literature (Motta et al. 2003; Qian et al. 1996). In Motta et al. (2003), a partitioned vector quantization is proposed in which the variable size partitions are determined adaptively, and the codebook of each partition was generated via the Linde-Buzo-Gray (LBG) algorithm (Linde et al. 1980). Huang et al. (2004a) develop the Differential Partitioned VQ (DPVQ) and Predictive Partitioned VQ (PPVQ) for the ultraspectal sounder data. Both schemes fall under the category of predictive vector quantization (Cuperman et al. 1982; Gersho et al. 1992). An open-loop design methodology is used such that the predictor is designed independently of the VQ codebooks. After the prediction step, the ultraspectral sounder data is partitioned spectrally based on the bit depth of each channel. Different vector quantizers are then designed for each partition using the LBG algorithm. The results for DPVQ and PPVQ are shown in Table 3. For comparison, the compression ratios of partitioned VQ (PVQ) on the complete granules are also shown. The PPVQ scheme significantly outperforms DPVQ and PVQ.

5. SUMMARY

The compression of ultraspectral sounder data is better to be lossless or near-lossless to avoid potential degradation of the geophysical retrieval in the associated ill-posed problem. In this paper, lossless compression of this data is performed using transform-based, prediction-based and clustering-based compression schemes. It is shown that the compression ratios of ultraspectral sounder data via the standard state-of-the-art algorithms (e.g. 3D SPIHT, 2D JPEG2000, 2D CALIC, 2D JPEG-LS etc.) can be significantly improved when combining the BAR preprocessing scheme. We also report the promising compression results for the ultraspectal sounder data using various approaches such as lossless PCA and Predictive Partitioned Vector Quantization (PPVQ).

Acknowledgement

The authors would like to thank Mitch Goldberg and Walter Wolf for providing the AIRS digital counts data. This research is supported by National Oceanic and Atmospheric Administration's National Environmental Satellite, Data, and Information Service under grant NA07EC0676. The views, opinions, and findings contained in this report are those of the authors and should not be construed as an official National Oceanic and Atmospheric Administration or U.S. Government position, policy, or decision.

References

ISO/IEC 14495-1 and ITU Recommendation T.87, 1999: Information Technology – lossless and near-lossless compression of continuous-tone still images.

ISO/IEC 15444-1, 2000: Information technology - JPEG2000 image coding system-part 1: Core coding system.

Abousleman G.P., M.W. Marcellin, and B.R. Hunt, 1997: Hyperspectral image compression using entropy-constrained predictive trellis coded quantization, *IEEE Transactions on Image Processing*, **6** (4), 566-573.

Abousleman G.P., 1999: Adaptive coding of hyperspectral imagery, *Proceedings of the 1999 IEEE International Conference on Acoustics, Speech, and Signal Processing,* 2243 -2246.

Aumann H.H., and L. Strow, 2001: AIRS, the first ultraspectral infrared sounder for operational weather forecasting, *Proceedings of IEEE Aerospace Conference*, 1683-1692.

Bloom H.J., 2001: The Cross-track Infrared Sounder (CrIS): a sensor for operational meteorological remote sensing, *Proceedings of the 2001 International Geoscience and Remote Sensing Symposium,* 1341-1343.

Canta G.R., and G. Poggi, 1998: Kronecker-product gain-shape vector quantization for multispectral and hyperspectral image coding, *IEEE Transactions on Image Processing*, **7** (5), 668-678.

Chang C.-I., and Q. Du, 1999: Interference and noise-adjusted principal components analysis, *IEEE Transactions on Geoscience and Remote Sensing*, **37** (5), 2387-2396.

Cuperman V., and A. Gersho, 1982: Adaptive differential vector coding of speech, *Conference Record GlobeCom 82*, 1092-1096.

Dragotti P.L., G. Poggi, A.R.P. Ragozini, 2000: Compression of multispectral images by three-dimensional SPIHT algorithm, *IEEE Transactions on Geoscience and Remote Sensing*, **38** (1), 416-428.

Eckstein, B.A., R. Peters, J.M. Irvine, R. Ritzel, R. Hummel, 2000: Assessing the performance effects of data compression for SAR imagery, *Proc. Appl. Imagery. Pattern Recog. Workshop*, 102-108.

Gersho A., and R.M. Gray, 1992: *Vector Quantization and Signal Compression*. Norwell, Mass: Kluwer Academic.

Hoffman R.N., and D.W. Johnson, 1994: Application of EOF's to multispectral imagery: data compression and noise detection for AVIRIS, *IEEE Transactions on Geoscience and Remote Sensing*, **32** (1), 25-34.

Huang, B., W. L. Smith, H.-L. Huang, and H. M. Woolf, 2002: Comparison of linear forms of the radiative transfer equation with analytic Jacobians, *Applied Optics*, **41** (21), 4209-4219.

Huang B., H.-L. Huang, H. Chen, A. Ahuja, K. Baggett, T. J. Schmit, and R. W. Heymann, 2003: Data compression studies for NOAA hyperspectral environmental suite using 3D integer wavelet transforms with 3D set partitioning in hierarchical trees, *SPIE Int. Symp. Remote Sensing Europe, Proc. of SPIE,* **5238**, 255-265.

Huang B., A. Ahuja, H.-L. Huang, T. J. Schmit, and R. W. Heymann, 2004a: Predictive partitioned vector quantization for hyperspectral sounder data compression, *SPIE Annual Meeting 2004, Proc. of SPIE,* **5548**, 70-77.

Huang B., H.-L. Huang, A. Ahuja, H. Chen, T.J. Schmit, R.W. Heymann, 2004b: Lossless data compression for infrared hyperspectral sounders – an update, *SPIE Annual Meeting 2004, Proc. of SPIE,* **5548**, 109-119.

Huang B., A. Ahuja, H.-L. Huang, T. J. Schmit, and R. W. Heymann, 2004c: Lossless compression of 3D hyperspectral sounding data using context-based

adaptive lossless image codec with Bias-Adjusted Reordering. *Optical Engineering,* **43** (9), 2071-2079.

Huang B., A. Ahuja, H.-L. Huang, T. J. Schmit, and R. W. Heymann, 2004d: Effects of the starting channel for spectral reordering on the lossless compression of ultraspectral sounder data, *SPIE International Asia-Pacific Symposium, 8-11 November, Honolulu, Hawaii.*

Lee H.S., N.-H. Younan, and R.L. King, 2000: Hyperspectral image cube compression combining JPEG 2000 and spectral decorrelation, *Proceedings of the IEEE International Geoscience and Remote Sensing Symposium (IGARSS)*, **6**, 3317-3319.

Linde Y., A. Buzo, and R.M. Gray, 1980: An Algorithm for Vector Quantizer Design, *IEEE Trans. Commun.*, COM-28, 84-95.

Mallat S, 1999: *A wavelet tour of signal processing*. Elsevier Academic Press.

Motta G., F. Rizzo, and J.A. Storer, 2003: Compression of hyperspectral imagery, *Proceedings of the 2003 IEEE Data Compression Conference*, 333-342.

Phulpin T., F. Cayla, G. Chalon, D. Diebel, and D. Schlüssel, 2002: IASI onboard Metop: Project status and scientific preparation,*12th Int. TOVS Study Conf., Lorne, Victoria, Australia*, 234-243.

Qian S.-E., A.B. Hollinger, D. Williams, and D. Manak, 1996: Fast 3-D data compression of hyperspectral imagery using vector quantization with spectral-feature-based binary coding, *Opt. Eng.*, **35** (11), 3242-3249.

Qian S.-E., A.B. Hollinger, M. Dutkiewicz, H. Tsang, H. Zwick, J.R. Freemantle, 2001: Effect of lossy vector quantization hyperspectral data compression on retrieval of red-edge indices, *IEEE Transactions on Geoscience and Remote Sensing*, **39** (7), 1459-1470.

Ryan M.J., and J.F. Arnold, 1998: A suitable distortion measure for the lossy compression of hyperspectral data, *Proceedings of the IEEE International Geoscience and Remote Sensing Symposium (IGARSS)*, **4**, 2056-2058.

Saghri J.A., A.G. Tescher, and J.T. Reagan, 1995: Practical Transform Coding of Multispectral Imagery, *IEEE Signal Processing Magazine*, **12** (1), 32-43.

Said A., and W.A. Pearlman, 1996: A new, fast, and efficient image codec based on set partitioning in hierarchical trees, *IEEE Trans. Circuits and Systems for Video Technology*, **6** (3), 243-250.

Shaw G. A., and H-h. K. Burke., 2003: Spectral Imaging for Remote Sensing, *Lincoln Laboratory Journal*, **14** (1), 3-28.

Shen S. S., J.E. Lindgren, P.M. Payton, 1993: Effects of multispectral compression on machine exploitation, *Twenty-Seventh Asimolar Conf. Signals, Systems, and Computers*, **2**, 1352-1356.

Smith W.L., F.W. Harrison, D.E. Hinton, H.E. Revercomb, G.E. Bingham, R. Petersen, and J.C. Dodge, 2002: GIFTS - the precursor geostationary satellite component of the future earth observing system, *Proceedings of the 2002 International Geoscience and Remote Sensing Symposium*, 357-361.

Tang X., S. Cho, and W.A. Pearlman, 2003: Comparison of 3D set partitioning methods in hyperspectral image compression featuring an improved 3D-SPIHT, *Proceedings of the 2003 IEEE Data Compression Conference*, 449.

Taubman D., 2000: High performance scalable image compression with EBCOT, *IEEE Transactions on Image Processing*, **9**, 1158-1170.

Wu X., 1997: Lossless compression of continuous-tone images via context selection, quantization, and modeling, *IEEE Transactions on Image Processing*, **6** (5), 656–664.

Granule 9	00:53:31 UTC	-12 H	(Pacific Ocean, Daytime)
Granule 16	01:35:31 UTC	+2 H	(Europe, Nighttime)
Granule 60	05:59:31 UTC	+7 H	(Asia, Daytime)
Granule 82	08:11:31 UTC	-5 H	(North America, Nighttime)
Granule 120	11:59:31 UTC	-10 H	(Antarctica, Nighttime)
Granule 126	12:35:31 UTC	-0 H	(Africa, Daytime)
Granule 129	12:53:31 UTC	-2 H	(Arctic, Daytime)
Granule 151	15:05:31 UTC	+11 H	(Australia, Nighttime)
Granule 182	18:11:31 UTC	+8 H	(Asia, Nighttime)
Granule 193	19:17:31 UTC	-7 H	(North America, Daytime)

Table 1. Ten selected AIRS granules for ultraspectral sounder data compression studies.

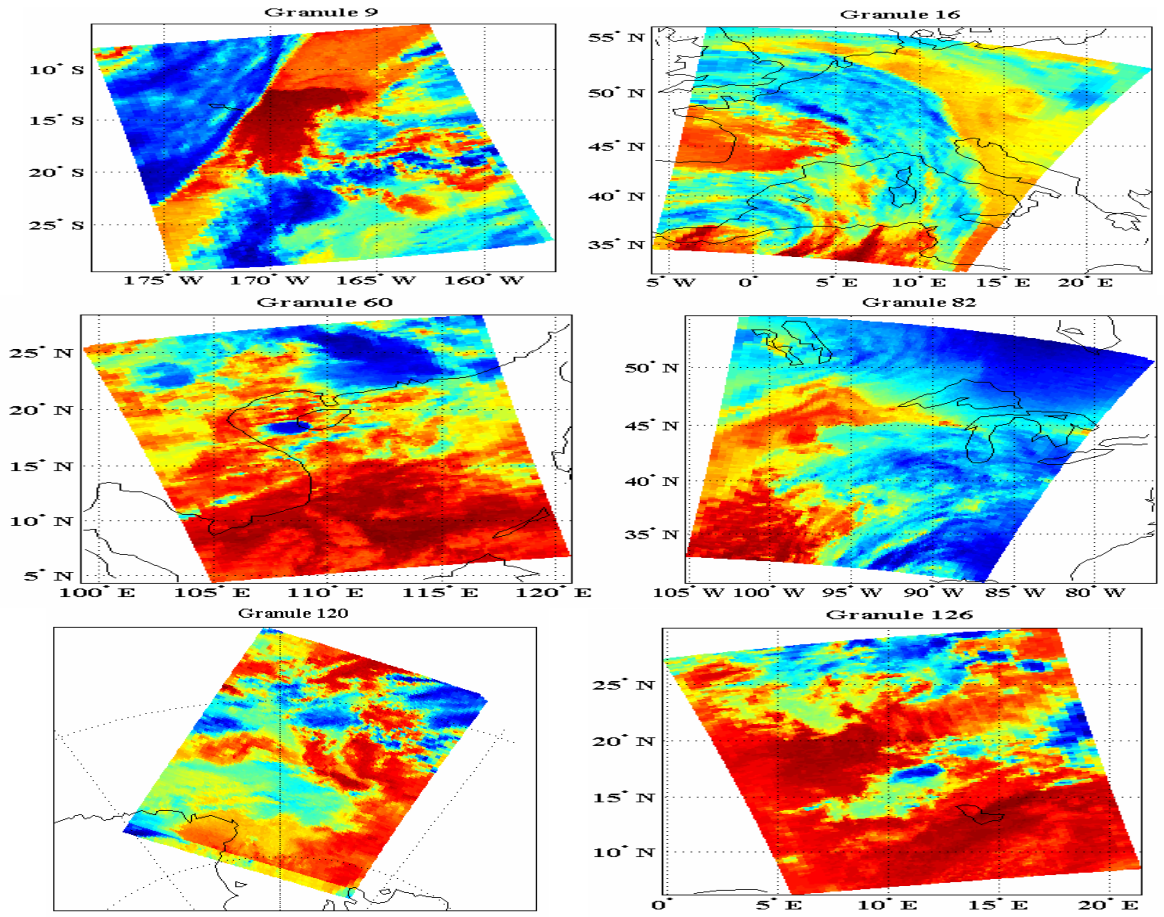

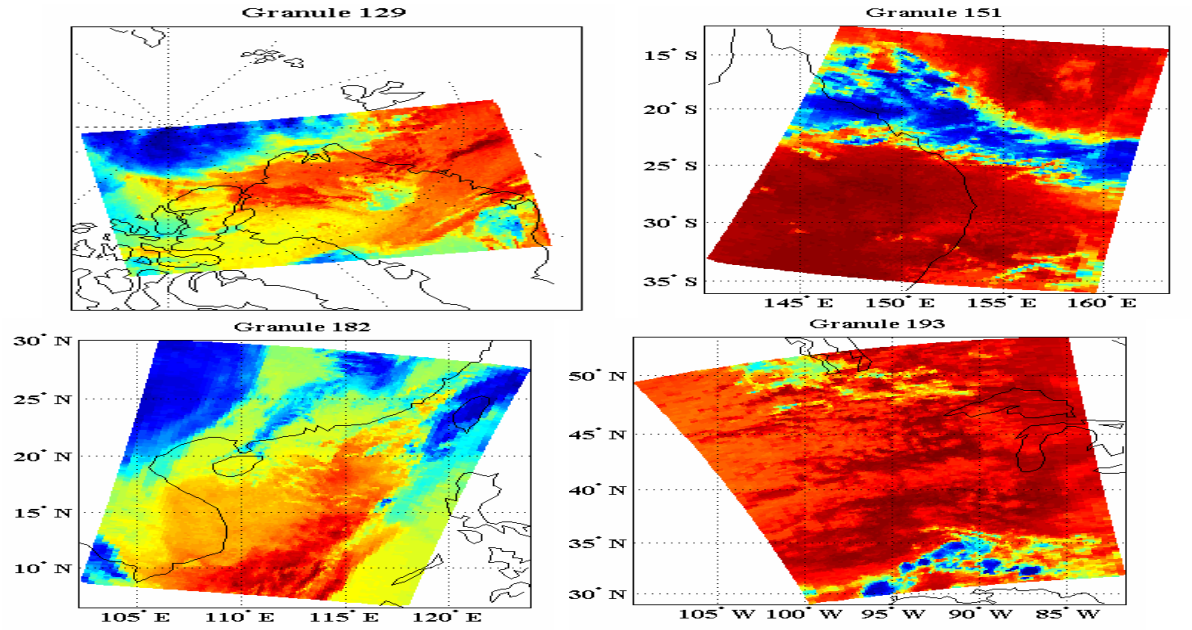

Figure 1. AIRS digital counts at wavenumber 800.01cm^{-1} for the 10 selected granules on March 2, 2004.

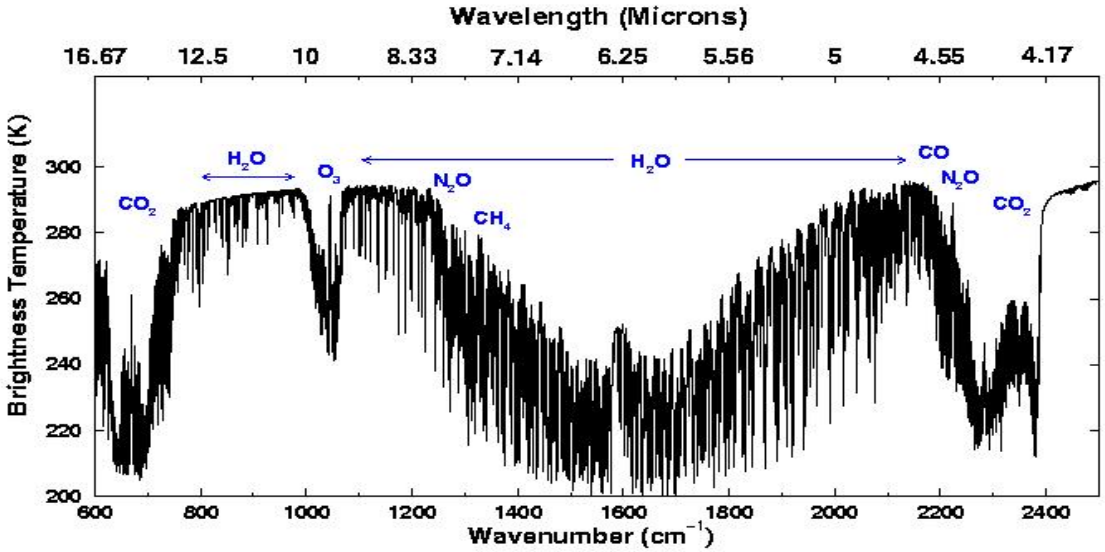

Figure 2. Dominant absorption gases in the infrared spectrum.

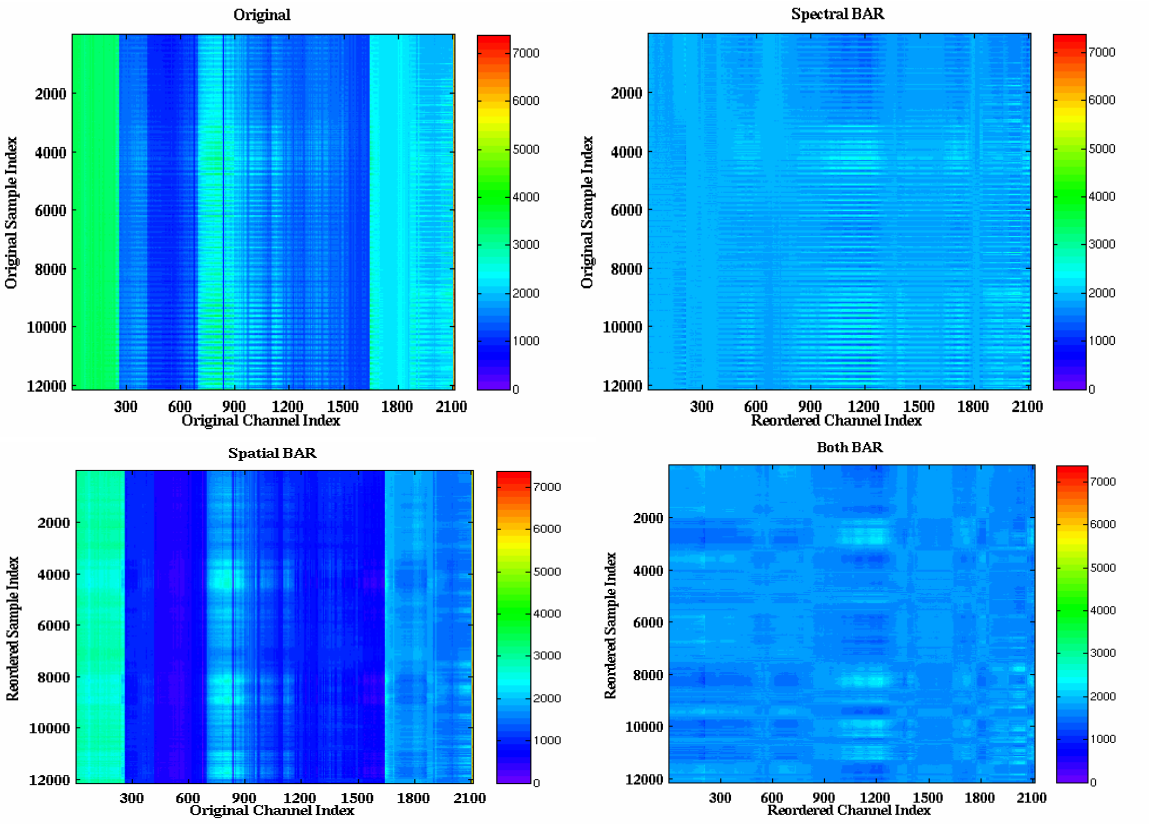

Figure 3. Example of 2D data distribution (a) of the original granule (b) after applying spectral BAR (b) after applying spatial BAR (d) after applying spectral BAR followed by spatial BAR.

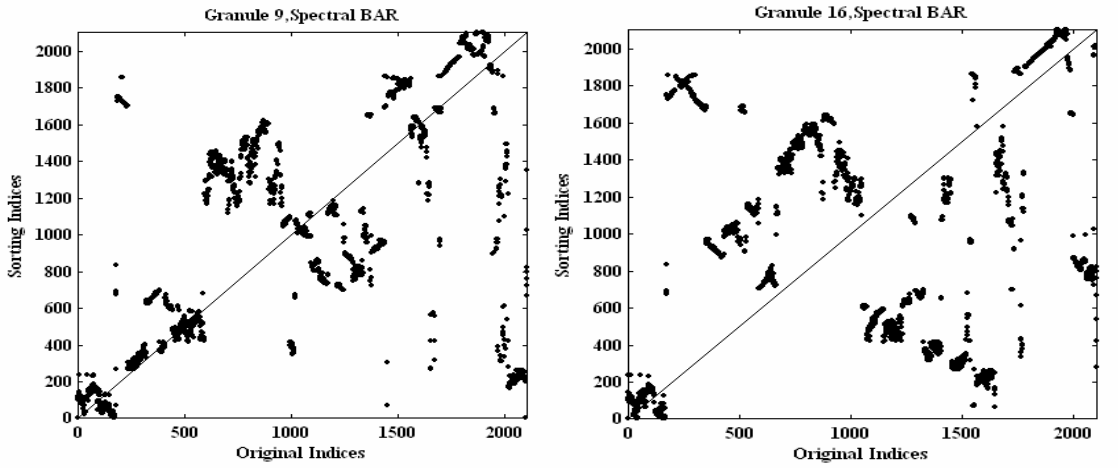

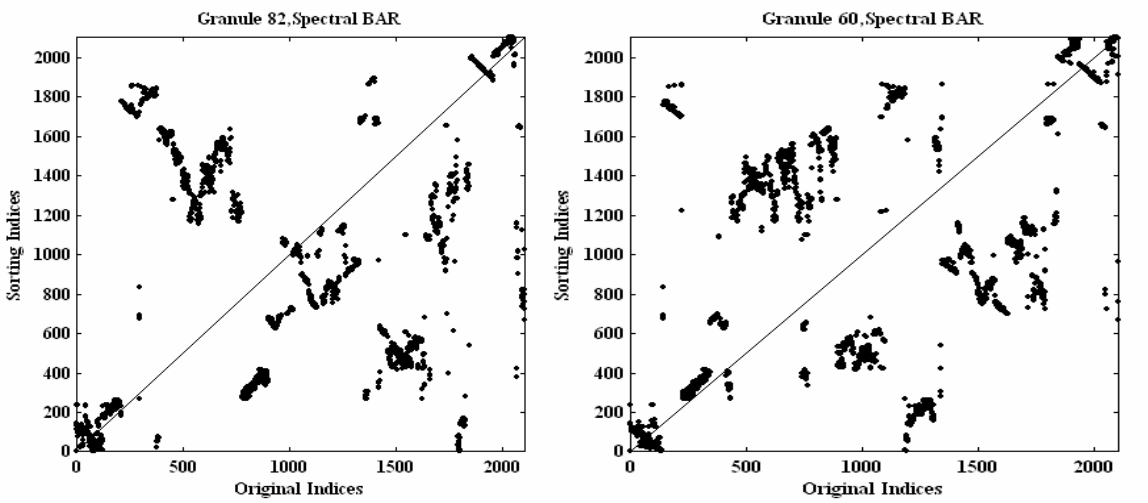

Figure 4. Spectral BAR sorting indices for various AIRS digital counts granules.

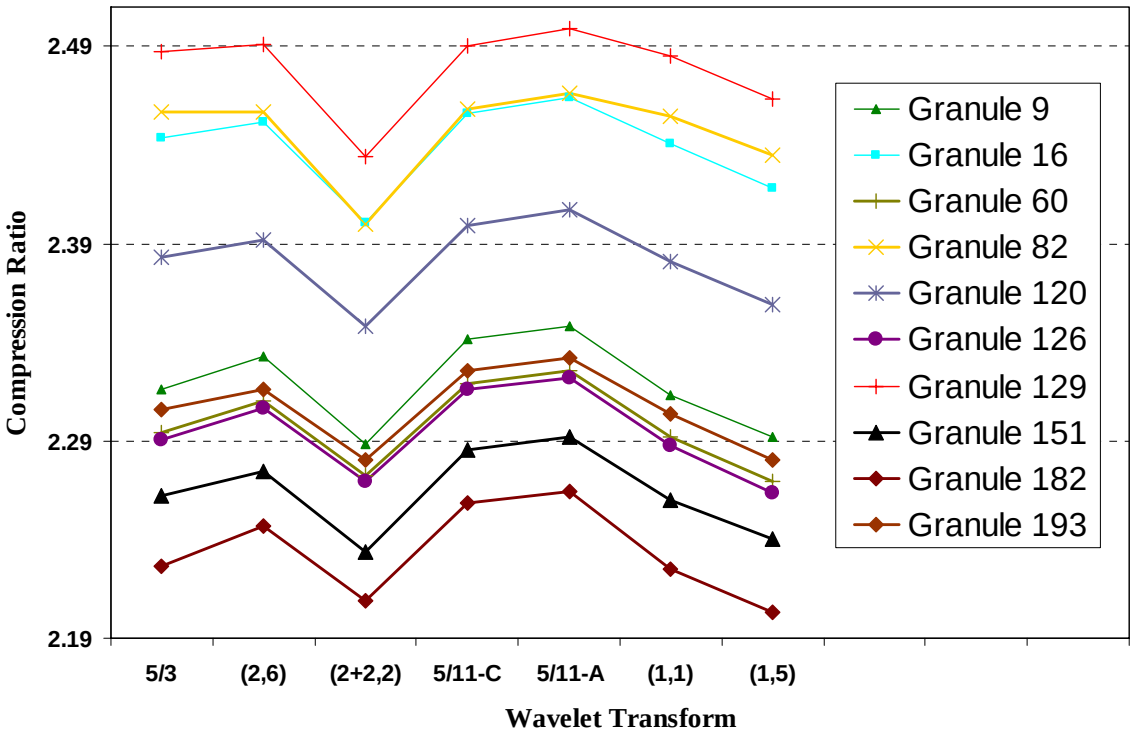

Figure 5. Compression ratios of ten granules using different wavelet transforms and 3D SPIHT.

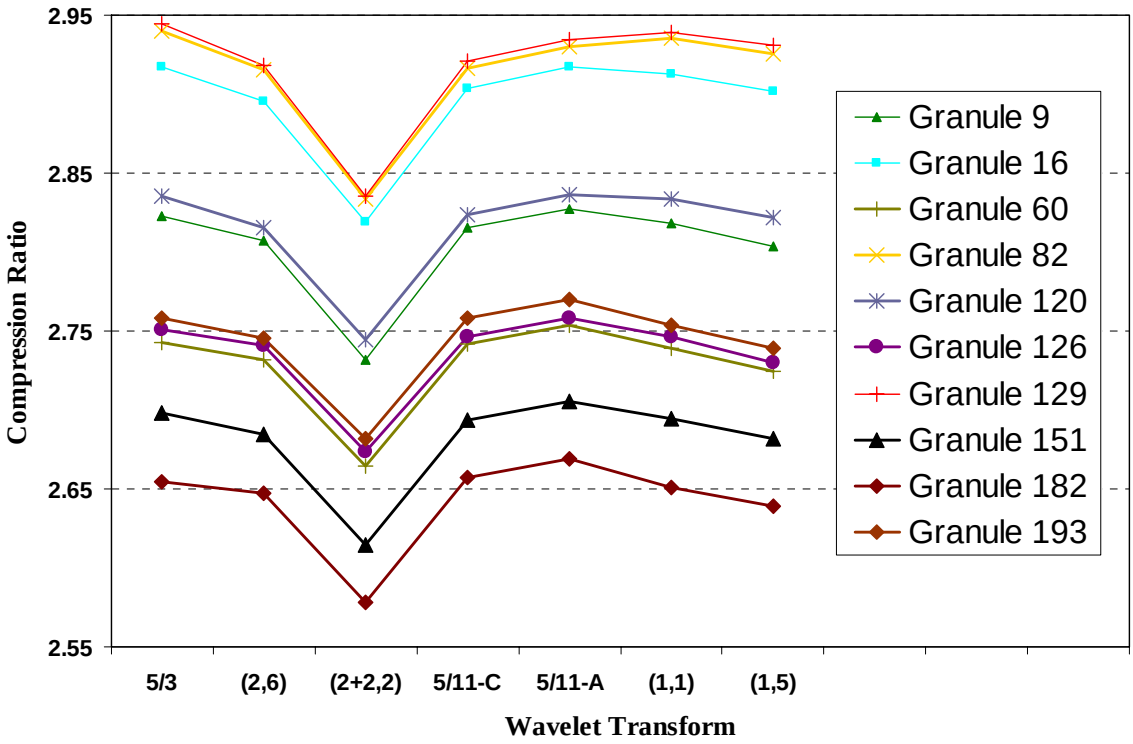

Figure 6. Compression ratios of ten granules after spectral BAR using different wavelet transforms and 3D SPIHT.

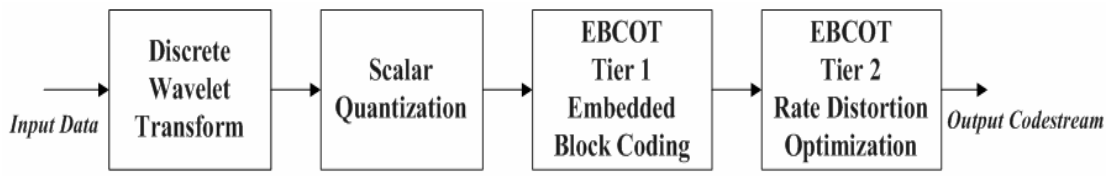

Figure 7. JPEG2000 encoder functional block diagram.

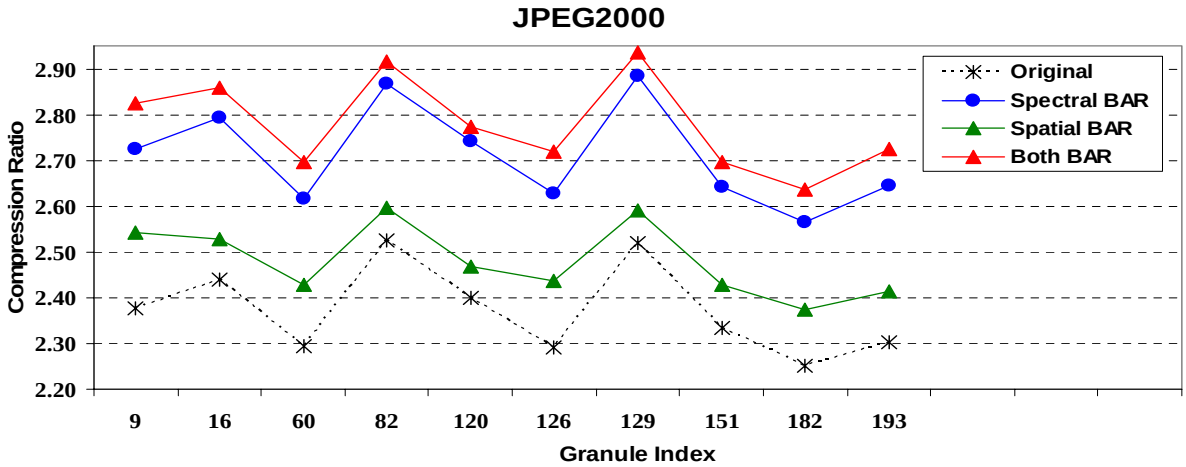

Figure 8. Compression ratios for JPEG2000 with and without BAR for ten tested granules.

Granule	full PCA
9	3.19
16	3.19
60	3.18
82	3.20
120	3.16
126	3.17
129	3.22
151	3.14
182	3.10
193	3.16
Average	**3.17**

Table 2. Compression ratios using Lossless PCA with 60 eigenvectors for ten granules.

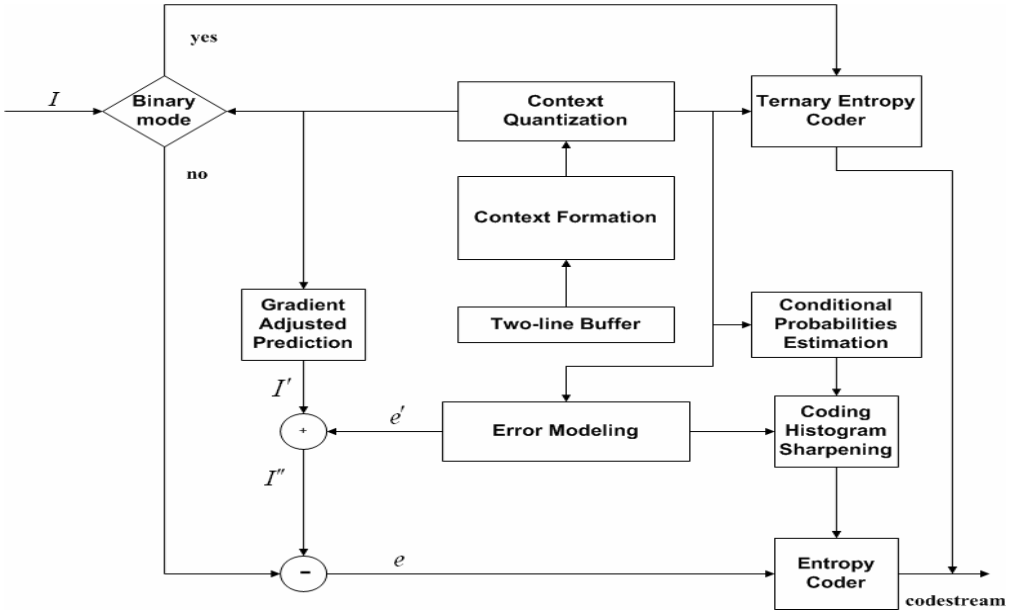

Figure 9. Schematic description of CALIC's encoder.

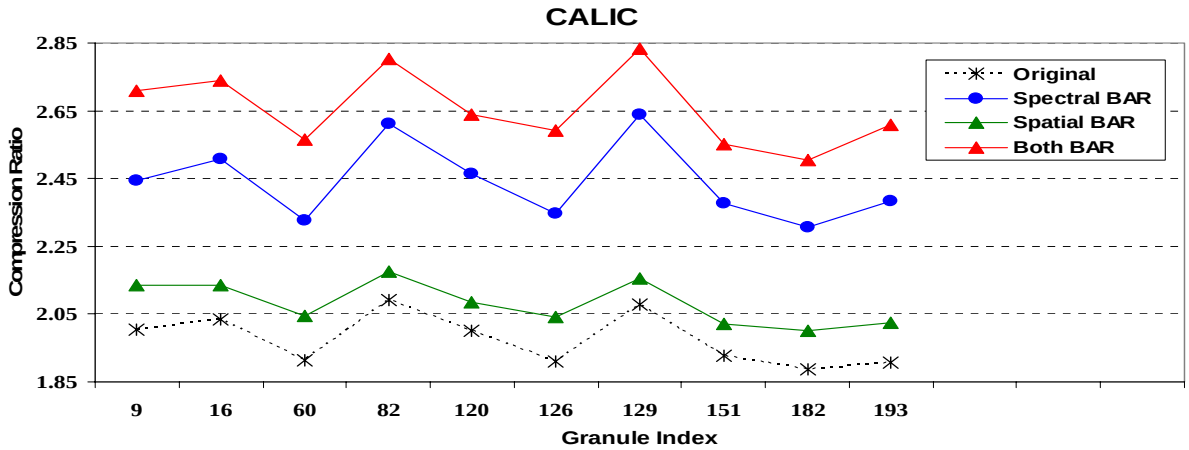

Figure 10. Compression ratios for CALIC with and without BAR for ten tested granules.

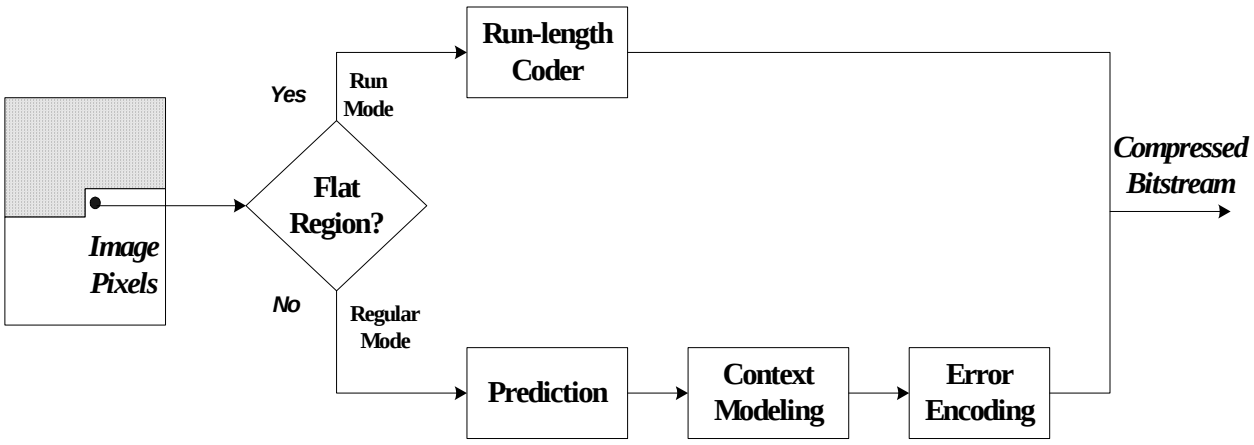

Figure 11. JPEG-LS encoder block diagram.

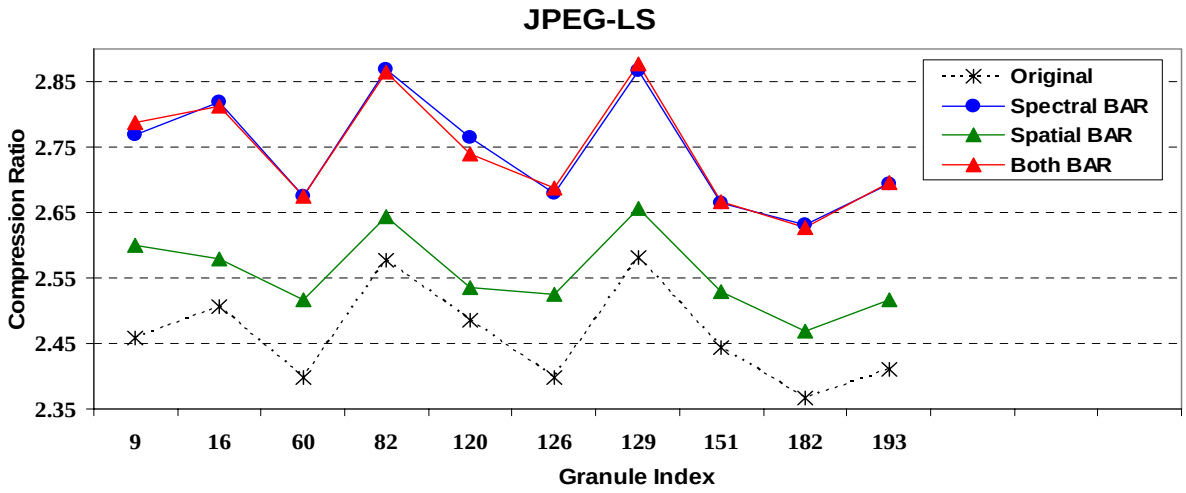

Figure 12. Compression ratios for JPEG-LS with and without BAR for ten tested granules.

Granule	PVQ	DPVQ	PPVQ
9	2.23	2.85	3.35
16	2.25	2.88	3.36
60	2.01	2.75	3.30
82	2.37	2.94	3.39
120	2.13	2.80	3.31
126	2.07	2.76	3.29
129	2.38	2.91	3.38
151	2.03	2.73	3.26
182	1.96	2.64	3.22
193	2.04	2.73	3.27
Average	**2.15**	**2.80**	**3.31**

Table 3. Compression ratios for partitioned VQ, DPVQ, and PPVQ on ten granules.